Available online at www.sciencedirect.com

SCIENCE DIRECT

Int. J. Electron. Commun. (AEÜ) 60 (2006) 179–189

International Journal AEÜ of Electronics and Communications

www.elsevier.de/aeue

Analytical spherical-mode-based compensation of mutual coupling in uniform circular arrays for direction-of-arrival estimation

Hendrik Rogier[a,*], Ernst Bonek[b]

[a] *Information Technology Department, Ghent University, St.-Pietersnieuwstraat 41, Ghent, Belgium*
[b] *Institut für Nachrichtentechnik und Hochfrequenztechnik, Technische Universität Wien, Gußhaustraße 25/389, Vienna, Austria*

Received 23 December 2004; accepted 3 February 2005

Abstract

An analytical circuit model with a limited number of parameters is presented to describe mutual coupling in uniform circular arrays. The model, which is based on a spherical-mode expansion, provides physical insight into the frequency dependence and the dependence on azimuth and elevation angle of the coupling between antenna elements. It is shown that the number of circuit elements, required to describe the open-circuit voltages and the mutual impedances at the different antenna ports, depends on the overall size of the array and not on the spacing between the antenna elements. Based on this observation, an analytical technique is described to derive a coupling matrix representing the mutual coupling effects. Relying on the phase-mode-based circuit elements, dedicated eigenstructure techniques are developed for direction-of-arrival (DOA) estimation with uniform circular arrays. By considering several synthetic reference scenarios, it is shown that even in the presence of severe mutual coupling, root-MUSIC combined with a limited number of phase-mode components gives very robust DOA estimations for the azimuth angle, when all signals are incident on the array from a fixed elevation angle.

Keywords: Antenna array mutual coupling; Array signal processing; Circular arrays; Mobile communication

1. Introduction

Antenna arrays play a key role in the development of high-performance mobile communications systems. Although a lot of theoretical work has been done on how the use of antenna arrays improves the system performance, relatively few contributions take into account the actual electromagnetic (EM) characteristics of the antenna system. Several authors, however, have shown that mutual coupling between antenna elements can drastically change the system behavior and its communication characteristics. This is due to a different EM behavior of the antenna elements in an array configuration, compared to their stand-alone characteristics, because of two important effects. First, terminal currents induced in the loads of neighboring elements introduce an extra voltage contribution in the antenna element under consideration. This effect is described by the impedance matrix $\overline{\overline{Z}}$. In [1], this impedance matrix is used to study the effect of mutual coupling on the performance of an adaptive linear array. A second important effect is the deformation of the radiation pattern of the stand-alone antenna elements due the detailed current distributions induced in the open-circuited neighboring antenna elements (shadowing effects) or neighboring scatterers (platform effects). As this effect occurs for a zero terminal current in the neighboring antenna elements, it only influences the diagonal elements

* Corresponding author. Tel.: +32 9 264 3343; fax: +32 9 264 3593.
E-mail address: hendrik.rogier@intec.ugent.be (H. Rogier).

1434-8411/$ - see front matter © 2005 Elsevier GmbH. All rights reserved.
doi:10.1016/j.aeue.2005.02.008

of the impedance matrix $\overline{\overline{Z}}$, but not the off-diagonal elements. Instead, for a receiving antenna array, the open-circuit voltage at a particular terminal, which results not only from the current distributions induced in the antenna element itself, but also from the induced current distributions of the open-circuited neighboring antenna elements and neighboring scatterers, then depends on the direction of the incoming signal, even if the array consists of omnidirectional standalone antenna elements. To accommodate for this second phenomenon as well, in [2] the concept of impedance matrix $\overline{\overline{Z}}$ is generalized to a coupling matrix $\overline{\overline{C}}$ to account for mutual coupling. Based on this approach, the multiple signal classification (MUSIC) algorithm is modified in [3] to take into account mutual coupling. As described in [4,5], in many cases the coupling matrix is able to compensate for mutual coupling. It is also demonstrated, however, that in some cases mutual coupling cannot be accounted for by means of a coupling matrix. This is especially so when platform effects play an important role. In [6–8], compensation of the mutual coupling effects in wire antenna arrays is performed by means of simulation data obtained by the Method-of-Moments (MoM), and in [9,10] numerical simulation data from full-wave [EM] solvers is applied to eliminate mutual coupling in planar and conformal arrays. In [11], an estimated current distribution is used to compensate for mutual coupling in arrays consisting of dipole elements and in [12], the mutual coupling is estimated together with the directions of arrival. The effect of mutual coupling on capacity of multi-element antenna systems is studied in [13–16].

In this paper, we construct an analytical circuit model describing mutual coupling effects in a uniform circular array (UCA). The classical circuit models for antenna arrays in transmit and receive mode, as reviewed in Section 2, do not allow to fully exploit the symmetries present in an UCA. By expanding the open-circuit voltages and the impedance matrix of the UCA into phase modes, introduced in [17], and spherical modes, we reduce the number of circuit elements in the model without reducing its accuracy, as shown in Section 2. The use of phase-modes allows to fully exploit the rotational symmetry in the UCA, both for the open-circuit voltage and the array impedance matrix contributions. It is shown that the number of circuit elements, required to describe the open-circuit voltages and the mutual impedances at the different antenna ports, depends on the overall size of the array but neither on the element spacing nor on the degree of mutual coupling between the antenna elements. In [18], dedicated eigenstructure techniques for direction-of-arrival (DOA) estimation with uniform circular arrays are considered, without taking into account mutual coupling effects. In Sections 3 and 4, these techniques are extended to include both mutual coupling phenomena described in Section 1. Existing techniques that compensate for mutual coupling using the impedance matrix $\overline{\overline{Z}}$, as in [1], or using the coupling matrix $\overline{\overline{C}}$, as in [2,3], have been proven to be inaccurate in certain cases. In [4,5], this problem is identified without further investigating the physical reasons. In this paper, however, it is shown that the problem is due to the second phenomenon described in Section 1: the deformation of the radiation pattern. Expanding the open-circuit voltage of the receiving antenna elements into spherical modes provides physical insight into this problem and allows to distinguish between cases for which compensation guarantees accurate results and the cases where radiation pattern deformation cannot be compensated. Therefore, in Section 5 we show how to construct a coupling matrix based on phase modes and we derive a criterion that shows that an accurate description is possible as long as the number of elements in the UCA is large compared to the largest electrical dimension of the array. The only assumption about the configuration is that the mutual coupling and the environment factors are rotationally invariant. In Section 6, the dedicated MUSIC algorithms and the use of a coupling matrix are applied for UCAs composed of dipole and dual-band dipole antenna elements. For the UCAs composed of dipole elements, we introduce a simple platform effect by placing a short-circuited dipole element in the center of the array. The effect of the electrical size of the array, the number of antenna elements, the impedance mismatch, and the frequency on DOA estimation techniques are investigated.

2. Describing the circuit model of a uniform circular array in terms of spherical modes

It is well-known that the EM behavior of an antenna in transmit mode is described by a radiation impedance, whereas in receive mode the antenna is characterized by the identical radiation impedance together with an open-circuit voltage source that depends on the radiation pattern of the antenna in transmit mode $\mathbf{F}_i(\theta, \phi)$ and the incoming field $\mathbf{E}^{\text{inc}}(\theta, \phi)$ [19, Chapter 2]. For antennas in an array configuration, additional mutual impedances appear in the circuit model describing mutual coupling. Explicitly, for a simple array consisting of two antenna elements in receive mode we obtain the circuit model shown in Fig. 1. Clearly, the system is completely characterized by a two-port impedance matrix $\overline{\overline{Z}}$ and a vector $\mathbf{V}_0$ containing the open-circuit voltage sources. The elements of the impedance matrix are found by exciting each port in turn with a 1A current source and measuring the voltage at that port as well as all open-circuit

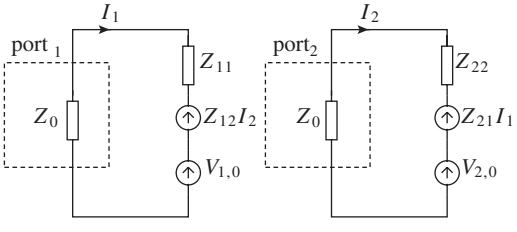

Fig. 1. Circuit models for a simple antenna array in receive mode.

voltages at the other ports. During the same process, a radiation pattern vector $\mathbf{F}_i(\theta, \phi)$ is obtained for each such excitation scheme. This radiation pattern is directly related to the open-circuit voltage $V_{i,0}$ in receive mode by [19, Chapter 2]

$$V_{i,0}(\theta, \phi) = -\frac{2\mathrm{j}\lambda}{R_\mathrm{c}}\mathbf{E}^\mathrm{inc}(\theta, \phi) \cdot \mathbf{F}_i(\theta, \phi), \tag{1}$$

where the vector $\mathbf{E}^\mathrm{inc}(\theta, \phi)$ represents an incoming plane wave at angles (θ, ϕ), where λ is the wavelength and R_c the impedance of the medium in which the antenna radiates. Note the angular dependence of the open-circuit voltages. This means that, in order to fully characterize mutual coupling in an array as a function of frequency, the impedance matrix must be known as a function of frequency as well as the open-circuit voltage vector, both as a function of frequency and as a function of all relevant angles of incidence. Note that the parameters used here to describe mutual coupling are related to arrays consisting of wire and patch antennes. However, by making use of duality, the concepts described here can be extended the UCAs of slot antennas as well.

Uniform circular arrays clearly exhibit a high degree of symmetry, which can be exploited to reduce the number of parameters in the circuit model for the array. We therefore make use of phase modes, as described in [17], and of spherical modes [20, Chapter 6]. To understand the physics behind these modes, we focus on a hypothetical multiport antenna that is defined by its current distribution $\mathbf{C}(r, \phi, z)$ on a surface S, being a circle with radius r. This current distribution can, for example, be computed by the NEC-2 code, for an array of wire antennas, thereby including all full-wave effects, such as mutual coupling. Let us for reasons of simplicity assume that the currents are z-oriented. Then, the z-oriented radiation pattern $F(\phi, \theta)$ is related to the current distribution by

$$F(\phi, \theta) = -\mathrm{j}\omega\mu_0 \sin\theta \int_{\phi'=0}^{2\pi}\int_z \Big[C(r, \phi', z) \times \mathrm{e}^{\mathrm{j}k_0(r\sin\theta\cos(\phi-\phi')+z\cos\theta)}\Big]\,\mathrm{d}\phi'\,\mathrm{d}z \tag{2}$$

with $k_0 = 2\pi/\lambda$, ω the angular frequency and μ_0 the free-space permeability. First, we deal with the dependence of the radiation pattern on azimuth and expand $F(\phi, \theta)$ into a Fourier series of phase modes [20, Chapter 5]

$$F(\phi, \theta) = \sum_{m=-\infty}^{+\infty} F_m^\phi(\theta)\mathrm{e}^{\mathrm{j}m\phi}. \tag{3}$$

The far field of the mth phase mode is then given by

$$\begin{aligned} F_m^\phi(\theta) &= -\frac{\mathrm{j}\omega\mu_0\sin\theta}{2\pi}\int_{\phi=0}^{2\pi}\int_{\phi'=0}^{2\pi}\int_z \Big[C(r, \phi', z) \times \mathrm{e}^{\mathrm{j}k_0(r\sin\theta\cos(\phi-\phi')+z\cos\theta)}\mathrm{e}^{-\mathrm{j}m\phi}\Big]\,\mathrm{d}\phi'\,\mathrm{d}z\,\mathrm{d}\phi \\ &= -\mathrm{j}^{m-1}\omega\mu_0\sin\theta J_m(k_0 r\sin\theta) \times \int_{\phi'=0}^{2\pi}\int_z C(r, \phi', z)\mathrm{e}^{-\mathrm{j}m\phi'}\mathrm{e}^{\mathrm{j}k_0 z\cos\theta}\,\mathrm{d}\phi'\,\mathrm{d}z. \end{aligned} \tag{4}$$

The latter relation has two important implications. First, the phase-mode component of the radiation pattern $F_m^\phi(\theta)$ is directly related to the phase-mode component of the same order in the current distribution $C(r, \phi', z)$ as the corresponding phase mode. Second, the amplitude of the coefficients $F_m^\phi(\theta)$ quickly decreases when the order m of the Bessel function J_m, corresponding to the angular mode number, is larger than its argument, thus when $m > k_0 r$.

In a second step, we deal with the dependence on elevation and expand the phase-mode coefficients $F_m^\phi(\theta)$ in the following series of associated Legendre polynomials $P_n^{|m|}(\cos\theta)$ [20, Chapter 6]:

$$F_m^\phi(\theta) = \sin\theta \sum_{n=0}^{+\infty} F_{m,n}^{\phi,\theta} P_n^{|m|}(\cos\theta). \tag{5}$$

The far field of the nth spherical mode is then given by

$$\begin{aligned} F_{m,n}^{\phi,\theta} &= -\mathrm{j}^{m-1}\omega\mu_0\int_{\phi'=0}^{2\pi}\int_z C(r, \phi', z) \\ &\times \left[\int_{\theta=0}^{\pi} J_m(k_0 r\sin\theta)\mathrm{e}^{\mathrm{j}k_0 z\cos\theta}P_n^{|m|}(\cos\theta)\sin\theta\,\mathrm{d}\theta\right]\mathrm{e}^{-\mathrm{j}m\phi'}\,\mathrm{d}\phi'\,\mathrm{d}z \\ &= (-1)^{\frac{n}{2}}(-\mathrm{j})^{m-1}\omega\mu_0\int_{\phi'=0}^{2\pi}\int_z C(r, \phi', z) \\ &\times j_n\left(k_0\sqrt{r^2+z^2}\right)P_n^{|m|}\left(\frac{z}{\sqrt{r^2+z^2}}\right) \\ &\times \mathrm{e}^{-\mathrm{j}m\phi'}\,\mathrm{d}\phi'\,\mathrm{d}z. \end{aligned} \tag{6}$$

Again, the amplitude of the coefficients $F_{m,n}^{\phi,\theta}$ quickly decreases when the order n of the spherical Bessel function j_n [20, App. D-20], corresponding to the spherical mode number, is larger than its argument, thus when $n > k_0\sqrt{r^2+z_\mathrm{max}^2}$. We conclude that the number of coefficients, $(2M+1) \times (N+1)$, required for expanding the radiation pattern of a circular array in spherical modes

$$F(\phi, \theta) = \sin\theta \sum_{m=-M}^{+M}\sum_{n=0}^{+N} F_{m,n}^{\phi,\theta} P_n^{|m|}(\cos\theta)\mathrm{e}^{\mathrm{j}m\phi} \tag{7}$$

is limited by the overall dimensions of the array both as a function of the angular index m and the spherical index n.

Consider a uniform circular array, consisting of N_e elements. We can measure or calculate the radiation pattern $\mathbf{F}_i(\theta, \phi)$ at one particular port. Probably, the pattern will be available as LK data samples along L uniformly distributed azimuth angles $\phi_l = 2\pi l/L$ and K uniformly distributed elevation angles $\theta_k = \pi k/K$. For each elevation angle θ_k, it

can first be decomposed into its phase-mode contributions by calculating

$$\mathbf{F}_{i,m}^{\phi}(\theta_k) = \frac{1}{L}\sum_{l=0}^{L-1} \mathbf{F}_i\left(\theta_k, \frac{2\pi l}{L}\right) \mathrm{e}^{-\mathrm{j}\frac{2\pi l m}{L}}, \tag{8}$$

which can be efficiently evaluated as a Fast Fourier Transform (FFT). Since for all elevation angles, the number of relevant coefficients is related to the array dimensions $k_0 r$, a limited number of terms in the phase-mode series will be sufficient to reconstruct the radiation patterns in small arrays that suffer from large mutual coupling effects. This results in a first reduction of the number of coefficients describing the mutual coupling. A second reduction is obtained by relying on symmetry. Indeed, once we know the series expansion for a certain port i, we can construct the radiation pattern at an arbitrary port p

$$\begin{aligned}\mathbf{F}_p(\theta, \phi) &= \mathbf{F}_i(\theta, \phi - \phi_p + \phi_i) \\ &= \sum_{m=-M}^{+M} \mathbf{F}_{i,m}^{\phi}(\theta)\mathrm{e}^{\mathrm{j}m(\phi-\phi_p+\phi_i)}.\end{aligned} \tag{9}$$

Finally, by applying the expansion (5), the continuous functions $\mathbf{F}_{i,m}^{\phi}(\theta)$ reduce to the discrete coefficients $F_{m,n}^{\phi,\theta}$, which are found by relying on the orthogonality of the associated Legendre polynomials and by performing numerical integration over the discrete samples $\mathbf{F}_{i,m}^{\phi}(\theta_k)$ along the elevation angles θ_k.

By the same procedure, we expand the open-circuit voltages into a series of spherical-mode voltages $V_{0,m,n}^{\phi,\theta}$

$$\begin{aligned}\mathbf{V}_{i,0}(\theta, \phi) &= \mathbf{V}_{1,0}(\theta, \phi - \phi_i) \\ &= \sin\theta \sum_{m=-M}^{+M}\sum_{n=0}^{+N} V_{0,m,n}^{\phi,\theta} P_n^{|m|}(\cos\theta)\mathrm{e}^{\mathrm{j}m(\phi-\phi_i)}.\end{aligned} \tag{10}$$

Similarly, all relevant voltages and currents are expanded following (10). By inserting these in the circuit model of Fig. 1, for each phase mode m the impedance matrix $\overline{\overline{Z}}$ reduces to the phase-sequence impedance Z_m^{ϕ}, given by

$$Z_m^{\phi} = \sum_{n=1}^{N_\mathrm{e}} Z_{i,n}\mathrm{e}^{-\mathrm{j}m\frac{2\pi(i-n)}{N_\mathrm{e}}}. \tag{11}$$

Because of symmetry, this impedance does not depend on a particular port i. The mutual coupling in a UCA is thus fully described by the phase-mode circuit model shown in Fig. 2. In this model, the phase-mode currents and voltages at the different ports are uncoupled for different mode orders m.

In order not to complicate things too much, we now concentrate on a fixed elevation angle θ. The relevant open-circuit voltages at that angle can always be found from the expansion of Eq. (10). Note then that an N_e element UCA is able to excite phase modes up to the order $\lfloor\frac{N_\mathrm{e}-1}{2}\rfloor$, by applying the correct amplitude and phase to the current sources

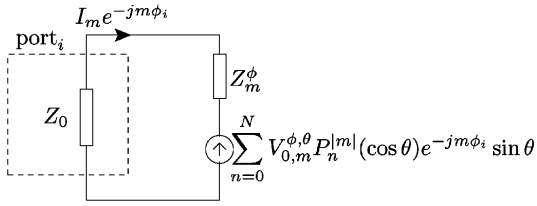

Fig. 2. Phase-mode circuit model of the UCA in receive mode, including mutual coupling.

at the different ports. The normalized beamforming weight vector that excites phase mode m is given by

$$\mathbf{w}_m^{\mathrm{H}} = \frac{1}{N_\mathrm{e}}\left[1, \mathrm{e}^{\mathrm{j}\frac{2\pi m}{N_\mathrm{e}}}, \ldots, \mathrm{e}^{\mathrm{j}\frac{2\pi(N_\mathrm{e}-1)m}{N_\mathrm{e}}}\right]. \tag{12}$$

The resulting radiation pattern

$$\mathbf{F}_m^{w}(\theta) = \sum_{k=-\infty}^{+\infty} \mathbf{F}_{1,m+N_\mathrm{e}k}^{\phi}(\theta)\mathrm{e}^{\mathrm{j}(m+N_\mathrm{e}k)\phi}$$

is not monomodal, however, since beside phase mode m, also modes with mode numbers $m+N_\mathrm{e}k$ ($k \in \mathbb{Z}$) are excited, in correspondence with Nyquist's sampling theorem. When the array fulfills $N_\mathrm{e} \gg k_0 r$, the contributions of higher-order modes, however, can be kept arbitrary small.

3. Real-beamspace MUSIC

Let us develop some specialized DOA-estimation technique for UCAs with mutually coupled antenna elements, using the phase-mode circuit model in receive mode derived in the previous section. In [18], dedicated eigenstructure techniques for uniform circular arrays were considered, without taking into account mutual coupling effects. Here, we use the reduced model described in Section 2 to extend these techniques when mutual coupling is important in uniform circular arrays.

Let us, for reasons of simplicity, start from an open-voltage situation: $\mathbf{a}(\theta, \phi) = \mathbf{V}_0(\theta, \phi)$. Whenever a load impedance Z_0 is present, one follows the same line of reasoning as below for deriving the real-beamspace MUSIC algorithm, but one replaces the phase-mode voltage $V_{0,m}$, corresponding to mode m, by $\frac{Z_0}{Z_0+Z_m^{\phi}}V_{0,m}$, with Z_m^{ϕ} given by Eq. (11). Furthermore, we assume that all signals are incident on the array from a fixed elevation angle θ. To transform the problem of DOA-finding from the element space to the beam space, we first apply the normalized beamforming weight vectors of Eq. (12), cast in the matrix $\overline{\overline{V}} = \sqrt{N_\mathrm{e}}\left[\mathbf{w}_{-M}\vdots\cdots\vdots\mathbf{w}_0\vdots\cdots\vdots\mathbf{w}_M\right]$. As discussed in the previous section, for N_e sufficiently large, application of this vector to an array manifold vector results in

$$\overline{\overline{V}}_0^{\phi}(\theta)\mathbf{v}(\phi) \approx \overline{\overline{V}}^{\mathrm{H}}\mathbf{V}_0(\theta, \phi) \tag{13}$$

with superscript T denoting transpose and H the conjugate transpose,

$$\mathbf{v}(\phi) = \left[e^{-jM\phi}, \ldots, e^{-j\phi}, 1, e^{j\phi}, \ldots, e^{jM\phi} \right] \tag{14}$$

and

$$\overline{\overline{V}}_0^{\phi}(\theta) = \mathrm{diag}\left[V_{0,M}^{\phi}(\theta), \ldots, V_{0,1}^{\phi}(\theta), V_{0,0}^{\phi}(\theta), V_{0,1}^{\phi}(\theta), \ldots, V_{0,M}^{\phi}(\theta) \right] \tag{15}$$

a diagonal matrix containing the phase-mode voltages. To develop a real-beamspace MUSIC algorithm as in [18], we now transform the vector $\overline{\overline{V}}_0^{\phi}(\theta)\mathbf{v}(\phi)$ into a centro-Hermitian vector [21], by premultiplying by the diagonal matrix

$$\overline{\overline{C}}_v(\theta) = \mathrm{diag}\left[e^{-j\angle V_{0,M}^{\phi}(\theta)}, \ldots, e^{-j\angle V_{0,1}^{\phi}(\theta)}, e^{-j\angle V_{0,0}^{\phi}(\theta)}, e^{-j\angle V_{0,1}^{\phi}(\theta)}, \ldots, e^{-j\angle V_{0,M}^{\phi}(\theta)} \right]. \tag{16}$$

Finally, the real-valued beamspace manifold is found by premultiplying by

$$\overline{\overline{W}} = \frac{1}{\sqrt{M'}} \left[\mathbf{v}(\alpha_{-M}) \vdots \cdots \vdots \mathbf{v}(\alpha_0) \vdots \cdots \vdots \mathbf{v}(\alpha_M) \right] \tag{17}$$

with $M' = 2M + 1$ and $\alpha_i = \frac{2\pi i}{M'}$. Applying all these different steps to the array manifold $\mathbf{a}(\theta, \phi)$ yields a real-valued beamspace manifold $\mathbf{b}(\theta, \phi)$ of the form:

$$\mathbf{b}(\theta, \phi) = \overline{\overline{W}}^{\mathrm{H}} \overline{\overline{C}}_v(\theta) \overline{\overline{V}}^{\mathrm{H}} \mathbf{a}(\theta, \phi) = \overline{\overline{F}}_r^{\mathrm{H}} \mathbf{a}(\theta, \phi) \tag{18}$$

$$= \left[f(\theta, \phi - \alpha_{-M}), \ldots, f(\theta, \phi - \alpha_{-1}), f(\theta, \phi), f(\theta, \phi - \alpha_1), \ldots, f(\theta, \phi - \alpha_M) \right] \tag{19}$$

with

$$f(\theta, \phi) = \sqrt{\frac{N}{M'}} \left[|V_{0,0}^{\phi}| + 2 \sum_{m=1}^{M} |V_{0,m}^{\phi}| \cos(m\phi) \right].$$

The beamspace MUSIC algorithm then proceeds as follows: let $s_l(t)$ correspond to the electric field strength of a signal impinging on the array from a DOA (θ, ϕ_l). When measuring the open-circuit voltages at the antenna terminals, we use (1) to find the N_e-dimensional vector of data samples $\mathbf{x}(t) = \sum_{l=1}^{L} \mathbf{v}_l(\theta, \phi_l) s_l(t) + \mathbf{n}(t)$, with L the number of sources, $\mathbf{v}_l(\theta, \phi_l)$ the array manifold vector and $\mathbf{n}(t)$ and additive white Gaussian noise component. In this contribution, at each antenna element the signal-to-noise ratio (SNR) is defined by

$$\mathrm{SNR} = \frac{E[|v_{0,1}(t)|^2]}{E[|n(t)|^2]}.$$

Thus, as the reference value for the signal contribution we take the mean square of the open-circuit voltage induced by an incoming plane wave with $|E_z| = 1$. We chose not to use the measured voltage over the load Z_0, represented by $|v_l(\theta, \phi_l)|$, in the definition of SNR, so that an antenna that has a severe mismatch with respect to the load Z_0 will also show bad performance. (We note in passing that the effect of a mismatch on the SNR is seldom taken into account in the implementation of signal processing algorithms for DOA estimation.) The vector $\mathbf{x}(t)$ is first transformed into the beamspace by applying the steps described above: $\mathbf{y}(t) = \overline{\overline{W}}^{\mathrm{H}} \overline{\overline{C}}_v(\theta) \overline{\overline{V}}^{\mathrm{H}} \mathbf{x}(t)$. The correlation matrix $\overline{\overline{R}}_y = E\left[\mathbf{y}(t)\mathbf{y}^{\mathrm{H}}(t)\right]$ is then computed and the signal and noise subspaces for its real part $\mathrm{Re}(\overline{\overline{R}}_y)$ are constructed by means of a real eigenvalue decomposition. The MUSIC spectrum is obtained in the classical way by projecting the real-valued beamspace manifold $\mathbf{b}(\theta, \phi)$ on the noise subspace.

4. Real-beamspace root-MUSIC

Whereas the standard MUSIC algorithm can be applied to very general arrays, its root-MUSIC implementation requires a well-defined structure in the array manifold, so that its straightforward implementation in the element-space is only feasible for uniform linear arrays in the absence of mutual coupling. For UCAs in the presence of mutual coupling, however, we can use the beamspace MUSIC technique derived in the previous section as a starting point for a root-MUSIC implementation in the beamspace. This root-MUSIC algorithm is applicable to UCAs even in the presence of mutual coupling. In the element space, the root-MUSIC algorithm can only be applied to uniform linear arrays. Let $\overline{\overline{G}}$ be an orthogonal matrix spanning the noise subspace, derived from a real eigenvalue decomposition of $\mathrm{Re}(\overline{\overline{R}}_y)$, as in Section 3. The DOAs then correspond to the minima of the function

$$\mathbf{v}^{\mathrm{H}}(\phi) \overline{\overline{V}}_0^{\phi,a}(\theta) \overline{\overline{WGG}}^{\mathrm{T}} \overline{\overline{W}}^{\mathrm{H}} \overline{\overline{V}}_0^{\phi,a}(\theta) \mathbf{v}(\phi) = \mathbf{v}^{\mathrm{H}}(\phi) \overline{\overline{Q}}(\theta) \mathbf{v}(\phi) \tag{20}$$

with

$$\overline{\overline{V}}_0^{\phi,a}(\theta) = \mathrm{diag}\left[|V_{0,M}^{\phi}(\theta)|, \ldots, |V_{0,1}^{\phi}(\theta)|, |V_{0,0}^{\phi}(\theta)|, |V_{0,1}^{\phi}(\theta)|, \ldots, |V_{0,M}^{\phi}(\theta)| \right]. \tag{21}$$

Since $\mathbf{v}(\phi)$ is given by (14), the null-spectrum can be written as

$$V(\phi, \theta) = \sum_{l=-M'+1}^{M'-1} a_\theta(l) e^{jl\phi} \tag{22}$$

with $a_\theta(l) = \sum_{i,j;\, j=i+l} \overline{\overline{Q}}_{i,j}(\theta)$. Setting $z = e^{j\phi}$ in (22) results in a polynomial equation, whose roots z_i that are close to the unit circle yield azimuth estimates for the DOAs: $\phi_i = \arg(z_i)$.

5. Constructing a coupling matrix based on phase modes

The use of a coupling matrix is a very popular way to represent mutual coupling in arrays. Often, this matrix is estimated by fitting the actual array response to the ideal array response at a number of discrete angles [4]. We will now present a procedure to derive the elements of a coupling matrix based on the phase-mode parameters of the UCA. Assuming that all signals arrive from the same elevation angle θ and that all antenna ports of the UCA are loaded by an impedance Z_0, we know that the voltage over the loads is given by (Fig. 1)

$$\mathbf{V}_{Z_0}(\phi,\theta) = Z_0(\overline{\overline{Z}} + Z_0\overline{\overline{I}})^{-1}\cdot\mathbf{V}_0(\phi,\theta). \tag{23}$$

An equivalent, but scalar, relation exists for the phase-mode voltages of order m (Fig. 2)

$$V^{\phi}_{Z_0,m}(\theta) = \frac{Z_0}{Z^{\phi}_m + Z_0}V^{\phi}_{0,m}(\theta). \tag{24}$$

Assume now that the response of an ideal array without mutual coupling is given by

$$\mathbf{V}^{(\mathrm{NC})}_{Z_0}(\phi,\theta) = V^{(1)}_0(\phi,\theta)\left(\mathrm{e}^{\mathrm{j}k_0 r\cos(\phi)}, \mathrm{e}^{\mathrm{j}k_0 r\cos(\phi-\frac{2\pi}{N_\mathrm{e}})}, \ldots, \mathrm{e}^{\mathrm{j}k_0 r\cos(\phi-\frac{2(N_\mathrm{e}-1)\pi}{N_\mathrm{e}})}\right)^{\mathrm{T}} \tag{25}$$

with $V^{(1)}_0(\phi,\theta)$ the open-circuit voltage of a stand-alone antenna element of the UCA or of a stand-alone reference antenna element such as a dipole. The ideal array manifold (25) can also be decomposed into phase-mode voltages $V^{\phi,(\mathrm{NC})}_{0,m}(\theta)$. As both the real and the ideal array have about the same size, the number of relevant phase modes is identical, only the way they are distributed differs. The correct distribution of phase modes for the real array can be reconstructed from the phase modes describing the ideal array manifold by loading the ideal array with an appropriate phase-sequence impedance for each phase mode. This means that, for each phase-mode m of the ideal array, we calculate a phase-sequence impedance $Z^{\phi,(\mathrm{MC})}_m$ by solving

$$V^{\phi}_{Z_0,m}(\theta) = \frac{Z_0}{Z^{\phi}_m + Z_0}V^{\phi}_{0,m}(\theta) = \frac{Z_0}{Z^{\phi,(\mathrm{MC})}_m + Z_0}V^{\phi,(\mathrm{NC})}_{0,m}(\theta). \tag{26}$$

This equation maps the ideal phase-mode voltages $V^{\phi,(\mathrm{NC})}_{0,m}(\theta)$ on the actual phase-mode voltage $V^{\phi}_{Z_0,m}(\theta)$. For an N_e element UCA, we are able to correct N_e mode components, i.e. $M = -\frac{N_\mathrm{e}-1}{2}, \ldots, \frac{N_\mathrm{e}-1}{2}$ when N_e is odd, or $M = -\frac{N_\mathrm{e}-2}{2}, \ldots, \frac{N_\mathrm{e}}{2}$ when N_e is even. Thus, we can correct mutual coupling with high accuracy by means of a coupling matrix, provided that $N_\mathrm{e} \gg k_0 r$. Once all relevant phase-sequence impedances for compensating the ideal array manifold are known, the compensating impedance matrix $\overline{\overline{Z}}_{\mathrm{MC}}$ is found by using an inverse discrete fourier transform (inverse of relation (11)). Finally, one obtains for the coupling matrix $\overline{\overline{C}}$

$$\mathbf{V}_{Z_0}(\phi,\theta) = \overline{\overline{C}}\cdot\mathbf{V}^{(\mathrm{NC})}_{Z_0}(\phi,\theta) = Z_0\left(\overline{\overline{Z}}_{\mathrm{MC}} + Z_0\overline{\overline{I}}\right)^{-1}\cdot\mathbf{V}^{(\mathrm{NC})}_{Z_0}(\phi,\theta). \tag{27}$$

6. Examples

6.1. An eight-port array of dipoles

Consider an eight-port array of thin dipole antennas tuned to 900 MHz (dipole length $l = 16.12$ cm). The array elements are distributed uniformly on a circle with diameter $d = l(\approx \frac{\lambda}{2})$. In [4], it is mentioned that for an array consisting of just dipoles, the mutual coupling is well represented by means of a coupling matrix. This is not the case when a short-circuited dipole with length $l = 16.12$ cm is added in the center of the circle. This element acts as a platform effect, as described in [4], and compensation of mutual coupling by means of a coupling matrix is not straightforward. Now choose the number of element ports $N_\mathrm{e} = 8$, in order to satisfy the criterion $N_\mathrm{e} > k_0\frac{d}{2}$ at 900 MHz, so that the real-beamspace MUSIC algorithm of Section 3 can be applied. To validate this statement, the spherical-mode voltages $|V^{\phi,\theta}_{0,m,|m|+n}|$ for the eight-element array are shown in Fig. 3. At 900 MHz, the most significant expansion coefficients are found in the region $|m| \leqslant 3$ and $n \leqslant 2$ and all relevant components are covered by choosing $M = 3$ and $M' = 7$.

To demonstrate the MUSIC algorithm, consider three uncorrelated sources emitting 10 000 bit pseudo-random bit sequences. All signals are incident along the xy-plane

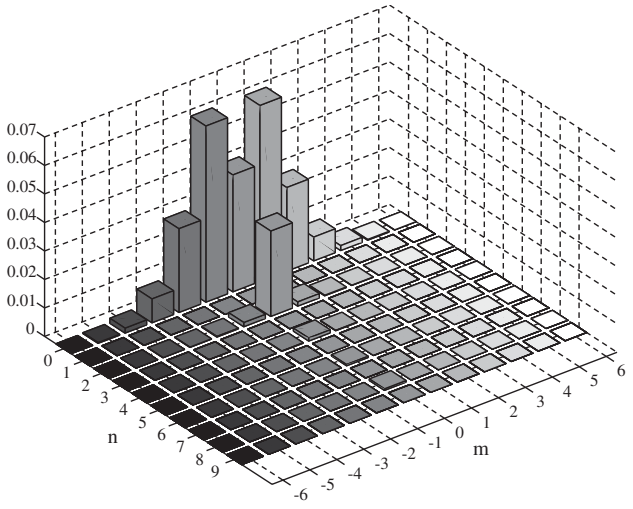

Fig. 3. Spherical-mode coefficients $|V^{\phi,\theta}_{0,m,|m|+n}|$ for the eight-element array at 900 MHz.

Table 1. Mean and standard deviation for DOA estimation at 900 MHz

SNR	MUSIC		RB-MUSIC		root MUSIC	
	3 dB	10 dB	3 dB	10 dB	3 dB	10 dB
DOA 1	55.0°(0.3°)	55.0°(0.0°)	55.1°(0.3°)	55.1°(0.1°)	55.0°(0.3°)	55.0°(0.1°)
DOA 2	96.0°(0.6°)	95.0°(0.1°)	95.3°(0.5°)	95.3°(0.2°)	95.3°(0.5°)	95.3°(0.2°)
DOA 3	143.0°(0.2°)	143.0°(0.0°)	143.2°(0.3°)	143.2°(0.1°)	143.2°(0.3°)	143.2°(0.1°)

Table 2. Resolving power at 900 MHz: incoming signals at 55° and 55° + δ, with SNR = 10 dB

δ	MUSIC		RB-MUSIC		root MUSIC	
	5°	10°	5°	10°	5°	10°
DOA 1	57.5°(1.4°)	55.3°(0.5°)	57.5°(1.9°)	55.2°(0.5°)	54.6°(1.4°)	54.9°(0.5°)
DOA 2	238.0°(22°)	64.7°(0.6°)	220.0°(55°)	64.3°(0.5°)	59.9°(1.2°)	64.6°(0.4°)

Table 3. Detection power at 900 MHz: incoming signals at 55° and 85°, with SNR = 30 dB

α	MUSIC		root MUSIC		RB-MUSIC	
	30 dB	40 dB	30 dB	40 dB	30 dB	40 dB
DOA 1	55.0°(0°)	55.0°(0°)	55.1°(0.02°)	55.1°(0.05°)	55.1°(0.0°)	55.1°(0°)
DOA 2	85.0°(0.6°)	120.0°(71°)	85.1°(0.5°)	85.4°(3.2°)	85.1°(0.5°)	85.1°(16°)

Power of second signal reduced by factor α compared to the first signal.

(elevation $\theta = 90°$). The signals are received in the presence of additive white Gaussian noise. We calculate the mean and standard deviation for an ensemble consisting of 500 implementations: in Table 1, for equally strong signals at DOAs $\phi_1 = 55°$, $\phi_2 = 95°$ and $\phi_3 = 143°$ at different SNR levels, in Table 2, for equally strong signals at DOAs $\phi_1 = 55°$ and $\phi_2 = 55° + \delta$ with SNR = 10 dB, and in Table 3 for signals at DOAs $\phi_1 = 55°$ and $\phi_2 = 85°$ with SNR = 30 dB and with the power of second signal reduced by factor α compared to the first signal. Throughout the manuscript the tables show the DOA estimates averaged over the ensemble under consideration. The value between brackets, behind each average value, is the standard deviation. Three implementations are considered: the (element-space) MUSIC algorithm, requiring full knowledge of the open-circuit voltages as a function of ϕ, for all ports, the real-beamspace algorithm, based on the knowledge of the phase-mode voltages for $m = -3, \ldots, 3$ and the root-MUSIC implementation described in Section 4. For the conventional MUSIC algorithm, the voltages were calculated with the NEC-2 code and listed in a table with a 1° angular resolution. This means that the conventional technique requires the knowledge of 8×360 parameters to describe the array manifold at that resolution. From this table, the phase-mode voltages were then computed by means of an FFT. The EM behavior of the array in the real-beamspace and the root-MUSIC implementation is characterized by 7 phase-mode voltages only. Still, the root-MUSIC algorithm discriminates DOAs with an angle separation of 5° and detects a DOA in the presence of another signal which is 40 dB stronger. In both these cases, the element-space MUSIC algorithm fails to detect both DOAs correctly. Furthermore, for the 500-element ensemble simulated in MatLab 6.5 on a 2.4 GHz Pentium IV processor, the real-beamspace algorithm (average Matlab runtime 48 s, where the average is taken over 20 Matlab runs) and the root-MUSIC implementation (average Matlab runtime 45 s, where the average is taken over 20 Matlab runs) were significantly faster than the element-space MUSIC approach (average Matlab runtime 55 s, where the average is taken over 20 Matlab runs). The latter technique also requires more storage, as 2880 parameters must be stored for each elevation angle, compared to 7 parameters for the beamspace approaches.

Let us now try to increase the detection performance and the resolving power of the array. In theory, this can be achieved by increasing the diameter of the array, or, equivalently, increasing the frequency. Consider the same array at 1800 MHz. Fig. 4 now shows that by choosing $M = 3$ and $M' = 7$, not all the relevant phase-mode voltage components are covered, since the relevant expansion coefficients are located in the region $|m| \leqslant 4$ and $n \leqslant 6$. This has an immediate effect on the accuracy of the DOA estimation. For example, when using the root MUSIC implementation to de-

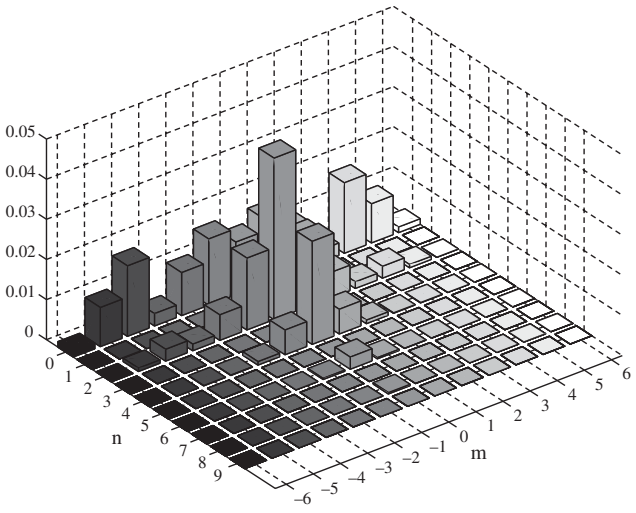

Fig. 4. Spherical-mode coefficients $|V^{\phi,\theta}_{0,m,|m|+n}|$ for the eight-element array at 1800 MHz.

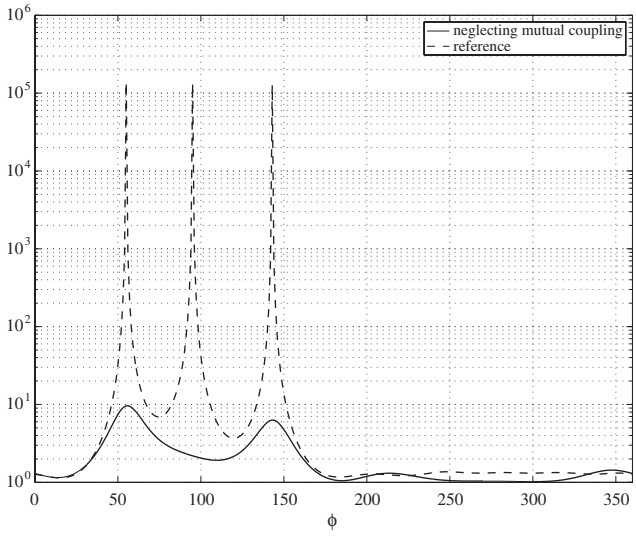

Fig. 5. MUSIC spectrum at 1800 MHz for nine antenna elements, not including mutual coupling.

tect equally strong signals at DOAs $\phi_1 = 55°$, $\phi_2 = 95°$ and $\phi_3 = 143°$ at SNR = 30 dB, a 500 element ensemble yields following average DOA estimates: $\phi_1 = 56.28°$, $\phi_2 = 99.08°$ and $\phi_3 = 145.93°$. Although the standard variation drops to 0.02, as a result of the increased electrical size of the array, biased results are obtained because of the inaccurate model for the mutual coupling. In contrast, the element space MUSIC algorithm, based on the complete knowledge of the array manifold gives correct estimates.

6.2. A nine-port array of dipoles

The accuracy of the real-beamspace MUSIC algorithm at 1800 MHz is much improved by adding an additional antenna element to the array, so that the algorithm can rely on the phase-mode voltages for $m = -4, \ldots, 4$. As one can verify in Fig. 4, the most relevant phase-mode voltages for describing the mutual coupling effects are now incorporated into our model. Now, the root-MUSIC implementation described in Section 4 yields the following ensemble averages for the DOAs estimates at SNR = 10 dB: $\phi_1 = 55.16°$, $\phi_2 = 95.09°$ and $\phi_3 = 143.00°$.

In order to get an idea on how inaccurate modelling of mutual coupling influences the DOA estimation, we now apply the real-beamspace MUSIC algorithm based on an array manifold that ignores mutual coupling, since it consists of the open-circuit voltages of the individual antenna elements in the absence of the other array elements. As a reference we again use the element-space MUSIC technique with the correct array manifold including mutual coupling effects. In Fig. 5 both MUSIC DOA spectra at 1800 MHz for a single implementation are shown. It is seen that by neglecting mutual coupling we fail to reconstruct the three DOAs.

The same effect is seen for the root-MUSIC algorithm, which gives following estimates for the DOAs: $\phi_1 = 54.9°$, $\phi_2 = 93.2°$ and $\phi_3 = 143.9°$. This clearly shows that neglecting the mutual coupling results in a severe loss of DOA estimation accuracy. The reason for this loss in accuracy in clearly seen in Fig. 6, where the phase-mode components are shown for an expansion in the azimuth plane ($\theta = 90°$). Although both in the presence and the absence of mutual coupling, the main contributions of the phase-mode voltages tend to concentrate between $m = -4$ and 4, mutual coupling clearly leads to a different distribution of the phase-mode components.

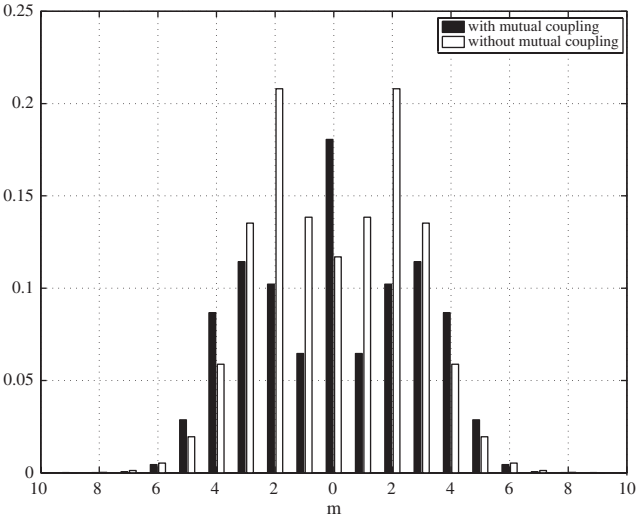

Fig. 6. Phase-mode voltages at $\theta = 90°$ for the array at 1800 MHz.

Let us now load all the antenna terminals with a termination $Z_0 = 73\,\Omega$. This represents a rather good match at $f = 900$ MHz, but a severe mismatch at $f = 1800$ MHz. To account for mutual coupling we either use the real-beamspace

Table 4. Nine-element UCA with $Z_0 = 73\,\Omega$: mean and standard deviation for DOA estimation

SNR = 10 dB	900 MHz				1800 MHz
	Open-circuit MUSIC	Comp. MUSIC	RB-MUSIC	root MUSIC	root MUSIC
DOA 1	39.0°(0.2°)	55.0°(0.2°)	55.0°(0.2°)	55.0°(0.2°)	36.5°(51°)
DOA 2	95.7°(0.5°)	95.0°(0.1°)	95.0°(0.3°)	95.0°(0.3°)	90.9°(15°)
DOA 3	157.1°(0.3°)	143.0°(0.04°)	143.0°(0.2°)	143.0°(0.2°)	142.0°(8°)

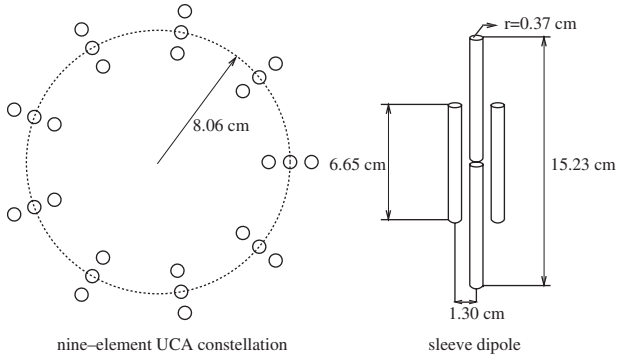

Fig. 7. Nine-element UCA consisting of dual-band dipole antennas.

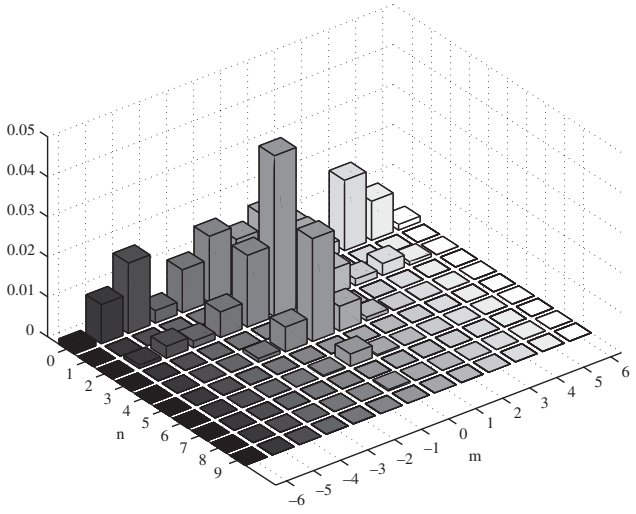

Fig. 8. Spherical-mode coefficients $|V^{\phi,\theta}_{0,m,|m|+n}|$ for the dual-band dipole array at 1800 MHz.

MUSIC approach discussed in Sections 3 and 4, or we construct a coupling matrix as described in Section 5 and use the element-space MUSIC algorithm. Moreover, these results are compared with the open-circuit voltage method described in [1]. In Table 4, the estimation of the three incoming signals is shown for different algorithms, at 900 and 1800 MHz and for SNR = 10 dB. At 900 MHz, all techniques presented in this paper, i.e. the compensated MUSIC approach, the real-beamspace and the root real-beamspace methods give accurate results. At this frequency, the coupling matrix in combination with the conventional MUSIC technique is able to compensate for mutual coupling. On the other hand, if one simply uses the open-circuit voltage method described in [1] to compensate for mutual coupling, one obtains rather inaccurate DOA estimates, proving that for this configuration, the open-circuit voltage method is not able to fully compensate for mutual coupling, even at 900 MHz. At 1800 MHz, due to antenna mismatch, both the conventional MUSIC algorithm compensated by the coupling matrix and the real-beamspace MUSIC approach fail to resolve the three signals. The root MUSIC technique resolves the three signals, but the accuracy is very poor.

6.3. An array of dual-band dipole antennas

Dipole antenna elements are relatively narrow-band, which can result in a severe impedance mismatch when using these elements to perform DOA estimation at different frequencies [6]. Therefore, more complex wire antennas should be used to cover multiple frequencies. In Fig. 7, we have tuned a dual-band dipole antenna to match 50 Ω at 900 and 1800 MHz ($S_{11} < -10$ dB). Let us first consider a UCA consisting of nine such antenna elements (Fig. 7). The antenna feeds are distributed uniformly on a circle of radius $r = 8.06$ cm, of identical size as for the nine-element dipole array in the previous subsection. Note, however, that the overall array dimensions are now slightly larger because of the dimensions of the dual-band dipole antennas. Even though the antenna elements are more complex than in the dipole array case, at 900 MHz, the most significant expansion coefficients are found in the region $|m| \leqslant 4$ and $n \leqslant 2$ and thus all relevant components are covered by choosing $M = 4$ and $M' = 9$. Again, at 1800 MHz, not all the relevant phase-mode voltage components are covered, as seen in Fig. 8, since the relevant expansion coefficients are then located in the region $|m| \leqslant 5$ and $n \leqslant 6$. Let us now load all antenna terminals with 50 Ω terminations and consider incoming signals in the azimuth plane. When constructing the coupling matrix, we use a stand-alone dipole antenna as a reference.

Consider two signals with equal power, incident at $\phi_1 = 55°$ and $\phi_2 = 65°$, with an SNR = 10 dB. At 900 MHz, mutual coupling can be compensated by a coupling matrix. This results in accurate average estimates for the compensated

Table 5. Dualband UCA: mean and standard deviation for DOA estimation at 1800 MHz: incoming signals at 55° and 65°, with SNR = 10 dB

N_e	root MUSIC			comp MUSIC		
	9	11	13	9	11	13
DOA 1	54.9°(0.6°)	55.2°(0.04°)	55.0°(0.03°)	—	56.0°(0°)	55.0°(0°)
DOA 2	65.1°(0.6°)	63.5°(0.06°)	65.0°(0.03°)	—	63.9°(0.3°)	65.0°(0°)

Table 6. Thirteen-element dualband UCA: mean and standard deviation for DOA estimation at 1800 MHz for incoming signals at 55° and 55° + δ, with SNR = 10 dB

δ	root MUSIC			
	2°	3°	4°	5°
DOA 1	55.8°(0.3°)	55.4°(0.6°)	55.8°(1.2°)	55.0°(0.02°)
DOA 2	57.0°(0.3°)	57.8°(0.5°)	58.2°(1.2°)	60.0°(0.02°)

element-space MUSIC when considering a 500-element ensemble: ϕ_1=55.02° and ϕ_2=64.97° and even slightly better average estimates for the root-MUSIC approach: ϕ_1=55.00° and ϕ_2 = 64.99°. Table 5 shows that, at 1800 MHz for a nine-element array, the compensated element-MUSIC algorithm is not able to resolve the DOAs, whereas the average DOA estimates are not so accurate at 1800 MHz when using the root-MUSIC approach. One can also observe in Table 5, however, a gradual increase in estimation accuracy when the number of elements increases.

When using 13 antenna elements, all relevant phase-mode components are covered. For this configuration, Table 6 shows that the root-MUSIC algorithm is able to accurately resolve DOAs down to an angle separation of 2°.

7. Conclusions

An expansion of the open-circuit voltages and the mutual impedances into phase modes and spherical modes was used to derive a rigorous circuit model with a limited number of parameters that describes mutual coupling in uniform circular arrays. The model provides physical insight on how mutual coupling between antenna elements depends on frequency, azimuth angle, and on the overall size of the array. It was shown that the number of circuit elements, required to describe the open-circuit voltages and the mutual impedances at the different antenna ports, depends on the overall size of the array. For a fixed overall size of the array, the number of circuit elements did not depend on the element spacing nor on the degree of mutual coupling between the antenna elements. Based on this observation, an analytical technique was described to derive a coupling matrix representing the mutual coupling effects. This technique can compensate for all mutual coupling and environment effects, provided they are rotationally invariant. Relying on the phase-mode-based circuit elements, dedicated eigenstructure techniques are developed for DOA estimation in such arrays. In the presence of antenna mismatch and of errors in modelling the mutual coupling effects, the root real-beamspace implementation in general provides more robust DOA estimates than the real-beamspace and the use of the coupling matrix together with the element-space MUSIC implementation. It is expected that the model for describing mutual coupling can also be combined with recently derived DOA estimation techniques, such as the rank-reduction (RARE) estimator [22] and the unitary root-MUSIC technique [23] for UCAs.

Acknowledgements

H. Rogier is a Postdoctoral Research Fellow of the FWO-V. His research was supported by a grant of the DWTC/SSTC, MOTION project and by a travel grant of the FWO-V.

References

[1] Gupta IJ, Ksienski AA. Effect of mutual coupling on the performance of adaptive arrays. IEEE Trans Antennas Propag 1983;31:785–91.
[2] Steyskal H, Herd JS. Mutual coupling compensation in small array antennas. IEEE Trans Antennas Propag 1990;38:1971–5.
[3] Friedlander B, Weiss AJ. Direction finding in the presence of mutual coupling. IEEE Trans Antennas Propag 1991;39:273–84.
[4] Su T, Dandekar K, Ling H. Simulation of mutual coupling effect in circular arrays for direction-finding applications. Microwave Opt Technol Lett 2000;26:331–6.
[5] Dandekar K, Ling H, Xu G. Experimental study of mutual coupling compensation in smart antenna applications. IEEE Trans Wireless Commun 2002;1:480–7.
[6] Pasala KM, Friel EM. Mutual coupling effects and their reduction in wideband direction of arrival. IEEE Trans Aerospace Electron Systems 1994;30:1116–22.
[7] Adve RS, Sarkar TK. Compensation for the effects of mutual coupling on direct data domain algorithms. IEEE Trans Antennas Propag 2000;48:86–94.
[8] Kim K, Sarkar TK, Salazar-Palma M. Adaptive processing using a single snapshot for a nonuniformly spaced array in the presence of mutual coupling and near-field scatterers. IEEE Trans Antennas Propag 2002;50:582–90.
[9] Rogier H, De Zutter D. Beamforming strategies for compact arrays using the exact active element pattern method. Microwave Opt Technol Lett 2002;35:202–3.

[10] Fernandez Recio R, Sarkar TK, Kim K. Elimination of mutual coupling in a conformal adaptive array antenna. IEEE AP-S Int Symp 2002;1:106–9.
[11] Hui HT. Improved compensation for the mutual coupling effect in a dipole array for direction finding. IEEE Trans Antennas Propag 2003;51:2498–503.
[12] Svantesson, T. Mutual coupling compensation using subspace fitting. Proceedings of the IEEE 2000 sensor array and multichannel signal processing workshop, Mar 2000. p. 494–8.
[13] Svantesson, T. Mutual coupling effects on the capacity of multielement antenna systems. Proceedings of the 2001 international conference on acoustics, speech, and signal processing, vol. 4, May 2001. p. 2498–503.
[14] Janaswamy R. Effect of element mutual coupling on the capacity of fixed length linear arrays. IEEE Antennas Wireless Propag Lett 2002;1:157–60.
[15] Wallace JW, Jensen MA. The capacity of MIMO wireless systems with mutual coupling, IEEE 2002 vehicular technology conference, VTC 2002-Fall-vol. 2, September 2002. p. 696–700.
[16] Waldschmidt C, Kuhnert C, Sörgel W, Wiesbeck W. MIMO-antennas in small handheld devices, 48. Internationales wissenschafliches kolloquium, TU Ilmenau, September 2003. p. 1–7.
[17] Davies DEN, The handbook of antenna design. In: Rudge A, Milne K, Olver A, Knight P (editors), London: Peregrinus; 1983 [Chapter 12].
[18] Mathews CP, Zoltowski MD. Eigenstructure techniques for 2-D angle estimation with uniform circular arrays. IEEE Trans Signal Process 1994;42:2395–407.
[19] Lo YT, Lee SW. Antenna handbook. New York: Van Nostrand Reinhold Company; 1988.
[20] Harrington RF. Time harmonic electromagnetic fields. New York: McGraw-Hill; 1961.
[21] Lee A. Centro-hermitian and skew-centro-hermitian matrices. Linear Algebra Appl 1980;29:205–10.
[22] Pesavento M, Gershman A, Wong K. Direction of arrival estimation in uniform circular arrays composed of directional elements, Proceedings of the second IEEE sensor array and multichannel signal processing workshop, vol. 50, 2002. p. 2103–115.
[23] Belloni F, Koivunen V. Unitary root-music technique for uniform circular array. 2003 IEEE international symposium on signal processing and information technology (ISSPIT 2003), December 2003.

Hendrik Rogier was born in 1971. He received the Electrical Engineering degree and the Ph.D. Degree from Ghent University, Gent, Belgium, in 1994 and in 1999, respectively.

He is currently a Postdoctoral Research Fellow of the FWO-V and a part time professor with the Department of Information Technology of Ghent University. He authored and co-authored about 25 papers in international journals and about 30 contributions in conference proceedings. He has one patent pending. His current research interests are the analysis of electromagnetic waveguides, electromagnetic simulation techniques applied to EMC and signal integrity problems, as well as to indoor propagation and antenna design, and in smart antenna systems for wireless networks. From October 2003 till April 2004 he was a visiting Research Fellow at the TU Wien, Austria.

Dr. Rogier received the URSI Young Scientist Award at the 2001 URSI Symposium on Electromagnetic Theory and at the 2002 URSI General Assembly.

Ernst Bonek was born in Vienna, Austria, in 1942. He received the Dipl.Ing. and Dr.Techn. degrees (with highest honors) from the Technische Universität Wien (TU Wien). In 1984, he was appointed Full Professor of Radio Frequency Engineering at the TU Wien. His field of interest is mobile communications at large. Recent contributions concern smart antennas, the characterization of mobile radio channels, and advanced antennas and receiver designs. His group pioneered 3D superresolution measurements of the urban mobile radio channel, the "double-directional" view point of the mobile radio channel, and propagation-based MIMO channel models. Previous fields of research were semiconductors, microwaves, optical communications, and intersatellite links. Altogether, he authored or coauthored some 170 journal and conference publications. He holds several patents on mobile radio technology. He coauthored the book Data Transmission over GSM and UMTS by Springer Verlag, and co-edited Technology Advances of UMTS by Hermes Scientific Publications.

From 1985 to 1990, he served the IEEE Austria Section as a Chairman. From 1991 to 1994 he was a council member of the Austrian Science Fund, acting as speaker for engineering sciences. From 1996 to 1999, he served on the Board of Directors of the reorganized Post and Telekom Austria. He participated in the European research initiative COST 259 as chairman of the working group on Antennas and Propagation, and continued to serve in this position in COST 273. In URSI, he was Chairman of Commission C "Signals and Systems" between 1999 and 2002. He is the initiator of FTW (Forschungszentrum Telekommunikation Wien), a public-private partnership for telecommunications research in Vienna, Austria. His industrial partners for contracted research include AKG, Alcatel SEL, austriamicrosystems, Elektrobit, e-plus, Kapsch, mobilkom austria, Nokia, NTTDoCoMo, Siemens, Telekom Austria, UNIDO. He was consultant/guest professor at ESA/ESTEC (Noordwijk, The Netherlands) in 1980/81, at TU Lulea (Sweden) in 1997 and with NTTDoCoMo (Yokosuka, Japan) in 2002.